

The ionization of carbon at 10-100 times the diamond density and in the 10^6 K temperature range.

M. W. C. Dharma-wardana*

National Research Council of Canada, Ottawa, Canada, K1A 0R6

(Dated: May 13, 2021)

The behaviour of partially ionized hot compressed matter is critical to the study of planetary interiors as well as for nuclear fusion studies. A recent quantum study of carbon in the 10-70 Gbar range and at a temperature of 100 eV used N -atom density functional theory (DFT) with $N \sim 32$ -64 and molecular dynamics (MD). This involves band-structure type electronic calculations and averaging over many MD generated ion configurations. The calculated average number of free electrons per ion, viz., \bar{Z} , was systematically higher than from a standard average atom (AA) quantum calculation. To clarify this offset, we examine (a) the effect of the self-interaction (SI) error in such estimates (b) the possibility of carbon being a granular plasma containing Coulomb crystals. The possibility of ‘magic-number’ bound states is considered. The electrical conductivity, pressure, and the compressibility of the carbon system are examined. The very low conductivity and the high \bar{Z} results of DFT-MD point to the existence of carbon in a complex non-uniform low-conducting dispersed phase, possibly containing magic-number Coulomb crystals. The NPA estimate of \bar{Z} , conductivity, compressibility, and pressure reported here pertain to the *uniform liquid*.

PACS numbers: 52.25.Jm, 52.70.La, 71.15.Mb, 52.27.Gr

I. INTRODUCTION

Astrophysics, planetary science and high-energy density physics rely heavily on theoretical predictions of the equation of state, transport and radiative properties as the information is not usually available experimentally [1]. The advent of short-pulse laser technology has also opened up new regimes of interest, where theoretical results are needed to interpret new experiments. Computational implementations of N -atom density functional theory (DFT) for electrons moving in the field of $N \sim 100$ –500 ions, coupled to molecular dynamics (MD) simulations for the ions have provided a reliable computational approach to these types of warm dense matter (WDM) [2, 3]. This DFT-MD approach will be referred to as the QMD method for brevity.

QMD provides the properties of the cluster of N -atoms modeled in the simulation cell as a periodic solid, but does not provide individual atomic properties unless additional steps are taken [4–6]. Such additional steps usually focus on decomposing density matrices, charge densities, N -atom energies, X-ray Thomson scattering scattering (XRTS), atomic phase shifts, N atom potentials, and such properties into one-atom properties or pair-atom properties, e.g., the pair potential [20]. However, Bethkenhagen et al. [7] have recently discussed the decomposition of a transport property, namely the electrical conductivity of highly compressed hot carbon, to determine the mean ionization state of the carbon atoms from a QMD N -atom calculation.

However, the application of the band-structure based approach to materials like carbon is subject to the well-known band gap error (BGE) which should affect any

determination of the number \bar{Z} of free electrons per ion that has been promoted over the band gap into the conduction band [8, 9]. Thus the fundamental gap of diamond, 5.48 eV, is underestimated by some 30% by typical DFT codes, while germanium in its insulator state ($\bar{Z} = 0$) is predicted to be a metal with $\bar{Z} = 4$. Similar BGE can be expected for the $1s$ -valance to conduction band energy gap in carbon relevant to the results of Ref. [7]. However, rectifying such errors using the GW method [9], applied in the 100 eV range for densities ρ at ~ 100 times the normal density would be computationally very prohibitive. Furthermore, alternative methods, e.g., average-atom (AA) methods also use DFT functionals that are subject to a similar self-interaction (SI) error.

The QMD method uses an electron XC-functional, $F_{ee}^{xc}[n]$ to reduce the many-electron quantum problem to a theory of non-interacting electrons, but explicitly deals with N -ions without reducing the N -atom problem further. Besides the N -atom DFT approach of QMD, the ‘one-atom DFT’, i.e., ‘average-atom’ (AA) methods directly yield ‘one-atom’ properties while taking account of the embedding medium in various approximations.

The metallic nature of typical WDMs has been exploited to construct a theory of these systems which is computationally very simple and yet flexible and accurate enough to provide useful results for astrophysically important low Z_n materials like C, N, Si etc., as well as for more general applications, using a complete density functional theory of matter where *both* the electron subsystem, and the ion subsystem are treated by DFT [10–14]. This approach also uses $F_{ee}^{xc}[n]$ to reduce the electron many-body problem to an effective one-electron problem. In addition, it reduces the many-ion problem to a one-ion problem using an ion-ion exchange correlation functional $F_{ii}^{xc}[\rho]$, dependent on the one-body ion density $\rho(r)$. Here the exchange component is negli-

* Email address: chandre.dharma-wardana@nrc-cnrc.gc.ca

ble in typical situations since ions can be regarded as classical particles. The Hohenberg-Kohn DFT for classical particles, needed in this approach for electron-ion systems is analogous to that for electrons and was discussed [10, 15, 16] soon after the development of the DFT treatment of electrons. The treatment of effects beyond the Born-Oppenheimer approximation requires an additional XC-functional $F_{ei}^{xc}[n, \rho]$. This is usually neglected but can be important in special circumstances, and for light ions [17]. In this full DFT approach the many-electron many-ion problem of many-body interactions is reduced to that of constructing an object consisting of an ‘‘average single ion of charge \bar{Z} plus \bar{Z} independent electrons’’, known as the neutral pseudoatom (NPA). The NPA uses XC-functionals to deal with three-body and such higher-order inter-particle effects. Thus the NPA is a ‘one-atom DFT’ approach which greatly simplifies the N -atom band-structure model that is implemented in the VASP, ABINIT and similar codes.

The NPA provides a calculation of the \bar{Z} , but it too is subject to a self-interaction correction (SIC) which is also the cause of the BGE in the band-structure approach. However, the simplified atomic physics model used in the NPA makes it easier to implement a SIC based on the Dyson equation [18, 19] or the method of Perdew and Zunger [8]. The XC-functionals for ions used, and the assumption of radial symmetry in the computational implementation of the NPA used here restricts the method to uniform systems.

Bethkenhagen et al [7] complemented their QMD results for the \bar{Z} of carbon with results from the Purgatorio AA code [30]. Intriguingly, the QMD results when decomposed to give the average degree of ionization of a single carbon atom showed a systematic overestimate of ~ 0.5 in the value of \bar{Z} compared to the AA \bar{Z} . We have calculated \bar{Z} using a Thomas-Fermi (TF) model, and our NPA method. The TF results is almost parallel to the QMD, with a 0.5 offset. The NPA finds a somewhat similar but more structured offset.

The objective of this study is to attempt to understand the magnitude of the likely SIC, and consider other possible reasons for the differences in the two types of estimates for \bar{Z} . Given the higher \bar{Z} found in the QMD, the reported extremely low conductivity from QMD using a Kubo-Greenwood calculation prompts us to consider that the QMD simulations, using $N = 32$ and 64, have converged on a region of the phase space where the plasma is granular, and possibly made up of Coulomb crystals. We suggest that various carbon clusters, each contributing about 0.5 electrons may form weak n, l, m bound states of a Coulomb crystal; the principle quantum number n is large enough to envelope the cluster. Filled shells are energetically favourable and \bar{Z} may increase to achieve this. These electronic ‘magic number’ states are further stabilized when clusters with N corresponding to a ‘structural’ magic number (e.g., $N = 13$) become possible simultaneously. This hypothesis fits in with the available results of the QMD and NPA calculations.

II. THE NPA CALCULATION OF \bar{Z}

Detailed discussions of the NPA may be found in several recent publications [20, 21]. In this study, the density $\bar{\rho}$, and temperature T (in energy units) are such that the carbon atom is found to carry only the $1s$ shell of bound electrons, providing a very simple model of an atom in a plasma. Hence, for simplicity of discussion we develop the two coupled DFT equations, i.e., for electrons and for the ions that are solved in the NPA, in the following simplified form where Hartree atomic units ($|e| = \hbar = m_e = 1$) are employed.

In our ‘one-atom’ DFT model, coupled equations resulting from the stationary condition of the grand potential $\Omega[n, \rho]$, considered as a functional of the one body electron and ion densities $n(r), \rho(r)$ are solved. A bare carbon nucleus of charge Z_n is the origin of coordinates of the uniform system of electrons and ions. Spherical symmetry is applicable, as we consider a uniform fluid. The inhomogeneous densities $n(r), \rho(r)$ around the carbon nucleus become the ‘bulk’ densities $\bar{n}, \bar{\rho}$ at large distances $r \rightarrow R_c$, where R_c is the radius of the ‘correlation sphere’. This is usually about ten Wigner Seitz radii. Here r_{ws} is given by $r_{ws} = \{3/(4\pi\bar{\rho})\}^{1/3}$. The pair-distribution functions (PDFs) $g_{ab}(r)$, $a = e, i$ refer to electrons or ions and describe the structure of the environment where the carbon atom is placed. Then

$$\rho(r) = \bar{\rho}g_{ii}(r), \quad n(r) = \bar{n}g_{ei}(r) \quad (1)$$

The PDF $g_{ii}(r)$ will be referred to as $g(r)$ for brevity. The grand potential can be written as

$$\Omega = T[N, \rho] + \Omega_e + \Omega_{ei} + \Omega_i. \quad (2)$$

Here $T[n, \rho]$ is the kinetic energy functional of a *noninteracting* system having the exact interacting densities. A simplified form for Ω_a is given below, assuming a point ion-model $U_{ei}(r) = -\bar{Z}/r$ for the electron-ion interaction. The more complete model, applicable even to ion mixtures is found in Ref. [11, 13] and used in the computations .

$$\Omega_e = - \int d\mathbf{r} \frac{Z_n}{r} n(r) + \frac{1}{2} \int d\mathbf{r} d\mathbf{r}' \frac{n(r)n(r')}{|\mathbf{r} - \mathbf{r}'|} \quad (3)$$

$$\int d\mathbf{r} F_{ee}^{xc}[n] - \mu_e \int d\mathbf{r} n(\mathbf{r}), \quad (4)$$

$$\Omega_{ei} = - \int d\mathbf{r} d\mathbf{r}' \frac{\bar{Z}\rho(r)n(r')}{|\mathbf{r} - \mathbf{r}'|} + \int d\mathbf{r} F_{ei}^{xc}[n, \rho] \quad (5)$$

Note that three-body and higher contributions beyond pair interactions are all contained in the XC-functionals, and are *not* neglected in the theory. That is, this one-atom DFT (viz., the NPA) does not use an external N -center potential energy surface due to the ions for the Kohn-Sham electrons, as is the case with the N -atom DFT deployed in VASP and ABINIT codes. What we have is the appropriate one-atom mapping of the N -atom DFT calculation.

We have used in Eq. 3 a point-ion model $-\bar{Z}/r$ for the electron-ion interaction of the field ions only for simplicity of presentation. In actual calculations a local pseudopotential $U_{ei}(q) = -\bar{Z}V_qM_q$, where $V_q = 4\pi/q^2$ and a form factor M_q are used. The form factor, and the corresponding ion-ion pair potential are also determined self-consistently from the NPA, as discussed elsewhere [11, 13, 20]. Non-local forms of the pseudopotential have not been found necessary for NPA calculations for uniform-density warm dense fluids or for cubic solids.

The ion contribution Ω_i can be obtained from the above equations by appropriately replacing $n(r)$ by $\bar{Z}\rho(r)$ if the ion-electron interaction is modeled by point ions, while also replacing F^{xc} contributions appropriately. The electron-ion XC-functional F_{ei}^{xc} is usually neglected in most NPA calculations, being largely equivalent to making the Born-Oppenheimer approximation, and neglecting certain correlation corrections of the form $\langle n(\mathbf{r})\rho(\mathbf{r}') \rangle - \langle n(r) \rangle \langle \rho(r') \rangle$. This is equivalent to using a ‘random-phase’ approximation for the electron-ion response function. This is appropriate for highly compressed *uniform* fluids of carbon studied here. However, such correlations may be important in dealing with composite carbon grains that form Coulomb crystals.

The stationary condition on Ω under functional variation δn leads to the usual Kohn-Sham (KS) equation for electrons moving in an effective potential $U_e(r)$. Functional differentiation with respect to $\delta\rho$ leads to an equation identifiable with the modified hyper-netted-chain (MHNC) equation if the ion-ion XC-functional is identified with the hyper-netted-chain (HNC) diagrams and bridge diagrams used for classical systems. The ions are classical in the regime of study, and there is no exchange contribution. Then the effective classical KS potential for the ions can be identified with the ‘potential of mean force’, $U_{ii}(r)$ (see appendix to Ref. [10]) of classical statistical mechanics.

In actual numerical work, the field ion distribution $\rho(r) = \bar{\rho}g(r)$ occurring in $\Omega_e(r), \Omega_{ei}(r)$ as well as in the corresponding KS equation $\delta\Omega/\delta n$ is replaced by $\bar{\rho}g_{cav}(r)$, where $g_{cav}(r)$ is a model ion-ion PDF which is just a spherical cavity of radius r_{ws} . Hence solving the electron KS equation coupled to the ion KS equation is much simplified, and the only parameter associated with the ion distribution that has to be varied self-consistently is the ion Wigner-Seitz radius r_{ws} appropriate to a given free electron density \bar{n} given as the input. Thus the primary input variable is the free electron density, for a given temperature and nuclear charge. The equilibrium ion density $\bar{\rho}$ is determined for each given \bar{n} in this manner, while solving the electron KS equation self-consistently, starting from a trial $n(r)$ and \bar{Z} .

The self-consistent solution for the continuum and bound state solutions is constrained to satisfy the Friedel sum rule and verified for satisfying the f -sum rule. The XC-functional used for the electron KS equation is the finite- T XC-functional of Perrot and Dharmawardana [22] within the local density approximation

(LDA). The XC-functional depends on T/E_F , where E_F is the Fermi energy of the free electrons. The electron system moves from a virtually classical ($T/E_F \sim 2$) electron gas to a strongly degenerate quantum gas ($T/E_F \sim 0.13$) in the system under study. A comparison of the finite- T XC-functional used here with the parametrization due to Dornheim et al [23] fitted to quantum Monte Carlo data showed good agreement [24]. The PBE electron XC-functional, i.e., at $T = 0$ has been used in the QMD calculations.

This partial decoupling of the electron Kohn-Sham equation and the ion Kohn-Sham equation used in the NPA implementation is possible because the electron Kohn-Sham equation is found to be only weakly dependent on the details of $g_{ii}(r)$ for $r > r_{ws}$. Furthermore, we use the free electron part of $n(r)$, viz., $n_f(r) = \bar{n} + \Delta n_f(r)$ obtained from the KS equation to construct the $\Delta n_f(r)$ that would be obtained if there were no $g_{cav}(r)$, using linear response (LR) theory. The corrected $\Delta_f n(r)$ is the response of a uniform electron fluid (in the presence of a non-responding neutralizing uniform ion background) to the carbon ion of charge \bar{Z} . Hence this corrected $\Delta n_f(r)$ may be regarded as being independent of the assumed form of $g(r)$ in solving the electron KS equation, as long as it satisfied basic criteria in regard to charge neutrality and the perfect screening sum rule.

Once the electron Kohn-Sham equation is solved using $g_{cav}(r)$, we already have the three quantities \bar{n}, \bar{Z} and hence $\bar{\rho}$. We also have the KS eigenfunctions $\phi_\nu(r)$ and eigenvalues ϵ_ν , with $\nu = n, l$ for bound states, and $\nu = k, l$ for continuum states, with $\epsilon_k = k^2/2$, together with the phase shifts δ_{kl} . These satisfy the Friedel sum rule and the simple charge neutrality condition $\bar{n} = \bar{Z}\bar{\rho}$. The DFT calculations used in the NPA also has the usual self-interaction error. Applying the SIC will make the NPA-estimate of \bar{Z} differ even more from the QMD, unless the QMD SIC is of the same magnitude. Nevertheless, we examine these corrections before attempting to discuss other reasons for the offset between our one-atom DFT results and those of Ref. [7].

III. RESULTS FOR \bar{Z} WITHOUT SELF-INTERACTION CORRECTIONS

The NPA model described in the previous section does not include self-interaction corrections. For instance, if the carbon atom has only the $1s$ bound state with one electron, with an energy ϵ_{1s} , its energy has been calculated with a KS-potential and a Coulomb repulsion inclusive of its own density. While the effect of this is correctly canceled out in the Hartree-Fock model of independent electrons, or in exact-exchange models, the simpler exchange correlation functionals do not contain the necessary XC-discontinuity needed to correct for the self-interaction. Hence new functionals that attempt to correct for the SIC exist [25], although their success is not as well established as for methods based on the Dyson

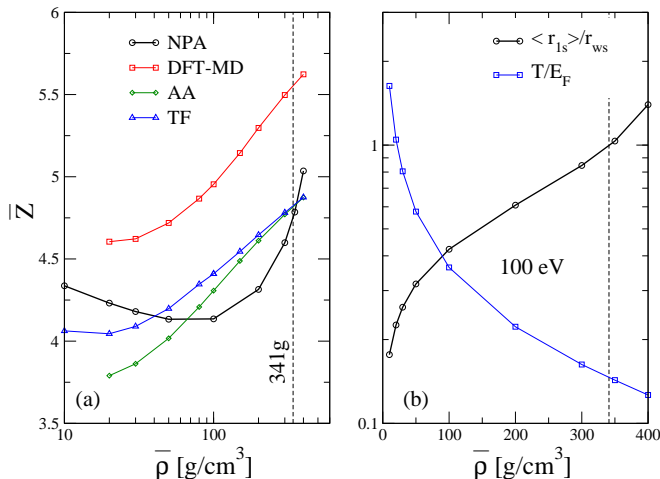


FIG. 1. (color online) Panel (a) \bar{Z} from several models. The results for the average atom (AA) and for DFT-MD are extracted from Ref. [7]. The \bar{Z} from the Thomas-Fermi model of More et al [26] are denoted by TF. The dashed vertical line labeled 341 g indicates the density (g/cm^3) where the mean radius of the $1s$ orbital becomes equal to the ion Wigner-Seitz radius. Panel (b) displays the effective ‘cooling’ of the system in terms of T/E_F , and the extension of the $1s$ orbital as the density is increased.

equation [9]. In this section we first examine the standard results from DFT-MD, the Purgatorio average-atom (AA) model as well as the NPA model, where no SIC has been used.

In fig. 1, panel (a) we display several calculations of \bar{Z} in the $\bar{\rho}$ range of interest, at 100 eV. No self-interaction corrections have been included. The Thomas-Fermi \bar{Z} used in the ‘Quotidian’ equation of state [26] is also displayed. The other models are discussed in more detail below.

A. DFT-MD band-structure model

In the N -atom DFT-MD model (QMD) the $1s$ electrons form a narrow ‘valance band’, while the continuum electrons form the ‘conduction band’ for each periodically repeated solid; i.e., the solid constructed via the MD evolution of the atomic positions in the simulation cell. Then an average over an ensemble of band configurations generated by MD is carried out, and the average ionization can in principle be calculated from the number of electrons per ion in the conduction band. The \bar{Z} can also be calculated from the one-atom decomposition of DFT-MD densities given by Plageman et al. [6]. Other methods of increasing sophistication for decomposing a ‘molecular property’ into ‘one-atom’ contributions are available [5].

A method based on the f -sum rule and the Kubo-Greenwood (KG) conductivity formula has been used in Ref. [7]. The method is applicable when there is a clear

separation of the conduction band and the valance band, without continuum resonances obscuring the bandgap. It would be worthwhile examining alternative decompositions of the N -atom properties that depend on \bar{Z} as well, unless a case can be made for the conductivity being the most satisfactory property for estimating \bar{Z} , even though DFT would require it to be estimated as a functional of the density.

The bandgap separating the top of the $1s$ band and the bottom of the conduction band, as well as the chemical potential of the electrons enter into the Kubo-Greenwood (KG) calculation of the conductivity that Bethkenhagen et al. [7] have used for extracting the number of free electrons per ion, i.e., \bar{Z} in their system. The band-gap error arises partly from the use of the KS eigenfunctions and eigenvalues whereas the solutions of the Dyson equation have to be used [9, 18] in KG. The bandgap error in the regime of densities and at 100 eV is unknown.

Encouragingly, consistent results have been obtained using the PBE [27] functional as well as the SCAN functional [28] in the work of Ref. [7]. Interestingly, the \bar{Z} from QMD is almost identical to that obtained from the Thomas-Fermi model, except for an increment $\Delta\bar{Z}=0.5$.

However, it should be noted that the Kubo-Greenwood (KG) formula when applied to the determination of the electrical conductivity of liquid-Si near and above its melting point using DFT-MD with the PBE functional or the SCAN functional does *not* lead to agreement with experiment. In the case of Si, there is excellent experimental data for the conductivity of liquid-Si in a small but technologically important range of densities, and hence a meaningful comparison is possible [21]. Many physical properties of liquid-Si predicted using DFT-MD seem to be sensitive to the XC-functional used [29]. Unfortunately, there are no experimental conductivities for carbon in this range of densities at 100 eV, or even for normal densities near the melting point to test these methods against experiment.

Hence calculations using other methods, and other codes are useful to determine the origin of the spread in the \bar{Z} found between the KG estimate and other theoretical approaches for \bar{Z} . Here we look at the results from the Purgatorio model and from the NPA model.

B. Purgatorio AA model

In contrast to the NPA, the Purgatorio model confines all the six electrons of the carbon atom within the WS cell (‘ion sphere’), and hence uses a μ different from the non-interacting μ^0 . The electron-ion interaction in the Purgatorio code is set to zero for $r > r_{ws}$. The self-interaction corrections should affect AA models in much the same way as for the NPA. According to [30], Purgatorio can be used to yield three estimates of \bar{Z} that converge towards the same value at sufficiently high T . The \bar{Z} given in Fig. 3 of Ref. [7] is stated to be obtained from the effective charge at $r = r_{ws}$. The \bar{Z} data, ex-

tracted from Ref. [7] is displayed in panel (a) of Fig. 1. It is seen that the results from the Purgatorio model converge towards the Thomas-Fermi model as the density is increased.

C. The NPA model

The NPA model has been used successfully for materials like Al, Si, Li etc., near their melting points and at much higher temperatures, unlike many AA models that seem to be designed mainly with high- T applications in mind. The NPA boundstates, as well as continuum states extend in the full volume of the correlation sphere, $R_c \sim 10r_{ws}$. The NPA differs from many AA models in that the electron-ion potential for $r > r_{ws}$ is not set to zero. The electron-ion potential becomes zero only outside the correlation sphere, $r \rightarrow R_c$. The corrections to μ^0 that are taken into account in elementary non-DFT theories of ‘continuum lowering’ etc., are included in the KS potentials that become zero only for $r > R_c$, when all the PDFs $g_{ab}(r)$, $a = e, i$ have attained the asymptotic value of unity.

The carbon NPA has only the single bound state, i.e., $1s$, under the conditions of the study. Hence the atomic potential is hard and almost point-like. Initially, at $\bar{\rho} = 20 \text{ g/cm}^3$ the electron chemical potential μ^0 is ~ -18 a.u.; that is, the continuum electrons are classical and hot, with $T/E_F \sim 1.7$ at 10 g/cm^3 . At lower densities, given the negative μ , electrons ionize easily and \bar{Z} is high. But as $\bar{\rho}$ increases, μ increases and becomes positive. The ionization is increasingly reduced until about 100 g/cm^3 . By then the mean radius of the $1s$ eigenstate of the carbon atom has reached 42% of the Wigner-Seitz radius, and reaches 61% by 200 g/cm^3 . Then the $1s$ state in the WS sphere begins to leak to the region outside the ion sphere; strong pressure ionization sets in, due to the potential of the ion subsystem modeled by $\bar{\rho}g_{cav}(r)$. The figure displays the density of 341 g/cm^3 when the $1s$ orbital radius becomes equal to r_{ws} .

In fact, one may consider that the effect of treating nearest neighbour interactions more explicitly, not only for this density, but from about $\bar{\rho}_{60} = 200 \text{ g/cm}^3$ may be important. If such nearest-neighbour $1s$ - $1s$ interactions are included, we obtain a narrow $1s$ -valance band averaged over the first peak of the ion-ion PDF. These would appear as transient bonding in MD simulations. This ‘valance band’ uses up electrons in the $1s$ states, but does not significantly change the estimate of \bar{Z} for the range of $\bar{\rho}, T$ studied here.

Nearest-neighbour interactions mediated via the continuum electrons are treated explicitly in the construction of the pair-potential that is employed to generate the actual $g(r)$. The resulting $g(r)$ differs significantly from $g_{cav}(r)$ outside the ion sphere. The actual $g(r)$ and the $S(k)$ are shown in Fig. 2.

The $g(r)$ and $S(k)$ are determined from a hyper-netted-chain calculation (or from MD if desired) using the ion-

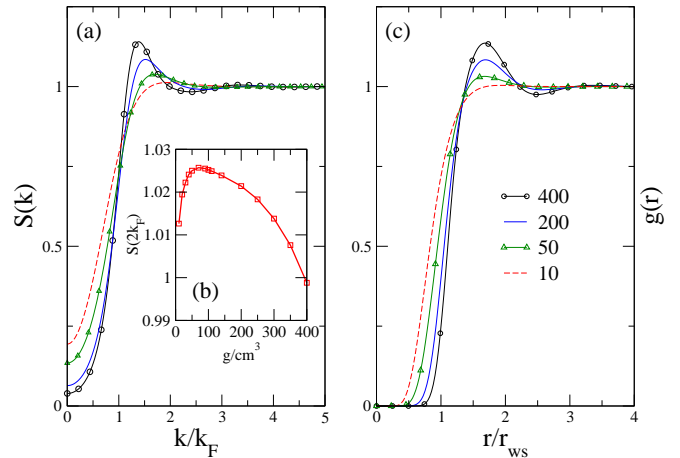


FIG. 2. (color online) Panel (a) The structure factors of liquid-carbon at 10, 50, 200 and 400 g/cm^3 are displayed. Unlike for normal densities (e.g. diamond $\sim 3.5 \text{ g/cm}^3$, the first peak is not split and shows no structure near $2k_F$. (b) This inset shows the variation of the value of $S(k)$ at $k = 2k_F$ which is determinative of the conductivity for $T/E_F < 1$. Panel (c). The C-C pair distribution functions has no subpeaks or structure due to bonding effects. The position of the first peak is typical of a densely packed uniform fluid.

ion pair potential defined via the NPA pseudopotential. The pseudopotential and the pair-potential used here are given by

$$U_{ei}(k) = \Delta n_f(k) / \chi(k, \bar{n}, T) \quad (6)$$

$$V_{ii}(k) = \bar{Z}^2 V_k + |U_{ei}(k)|^2 \chi(k), \quad V_k = 4\pi/k^2. \quad (7)$$

Here $\Delta n_f(k)$ is the Fourier transform of the free-electron density displacement around the nucleus of the carbon atom placed in the medium with average ion density $\bar{\rho}$ at T . The fully interacting response function of the electron fluid is denoted by $\chi(k, \bar{n}, T)$, and abbreviated to $\chi(k)$, while V_k is the Coulomb potential. The response function uses a finite- T local field correction whose $k \rightarrow 0$ is chosen to satisfy the compressibility sum rule.

D. The effect of self-Interaction corrections on \bar{Z}

DFT calculations do not normally include a self-interaction correction. So we include such a correction although we recognize that this may not resolve the difference between the QMD-prediction and the NPA prediction. The inclusion of a SIC makes the XC-functional not only a functional of the density $n(r)$, but also explicitly dependent on the orbital wavefunction.

We use the model of Perdew and Zunger [8] rather than the Dyson equation approach [18]. In this model, the average value of the Coulomb potential $U(n_\alpha)$ for the electron density in the orbital α, σ under consideration, and its XC-potential are added together and subtracted from the uncorrected Kohn-Sham eigenvalue. The expression

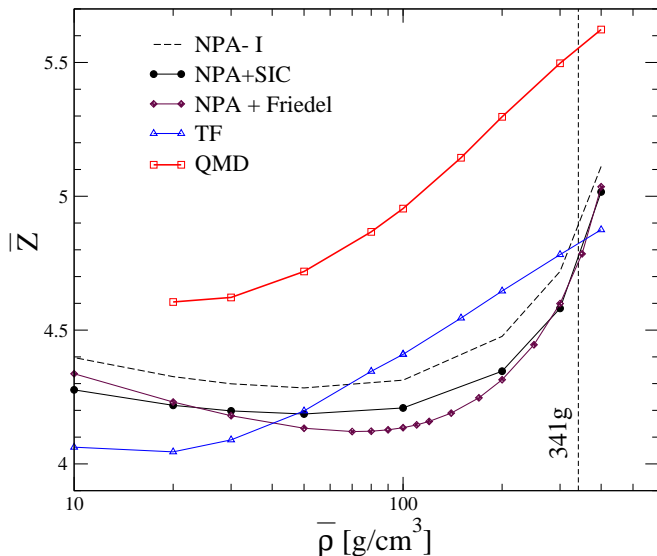


FIG. 3. (Color online) The NPA estimate of the mean number of free electrons per ion, i.e., \bar{Z} , is given in successive estimates. NPA-I is the ‘naive’ estimate, based on the $1s$ occupation number. This is then corrected for the self-interaction error. The calculation imposing the Friedel sum rule is also given. So the estimate is well-contained and uncertainties in the NPA- \bar{Z} are definitely smaller than the offset from the QMD estimate. The Thomas-Fermi \bar{Z} is shown for comparison. The SC has been evaluated following Perdew and Zunger [8].

is most clearly written in the language of spin-density functionals. Given a spin density-functional orbital $\phi_{\alpha,\sigma}$ containing an electron density $n_{\alpha,\sigma}$, and the fully spin-polarized XC-potential $V_{xc}[n_{\alpha\sigma}, 0]$, the SIC is given as:

$$\Delta\epsilon_{sic} = -\langle\phi_{\alpha\sigma}|U(n_{\alpha,\sigma}(r) + V_{xc}[n_{\alpha\sigma}(r), 0])|\phi_{\alpha,\sigma}(r)\rangle \quad (8)$$

Here $\phi_{\alpha,\sigma}(r)$ is the eigenfunction obtained by self-consistently solving the KS equation including the SIC in it. This equation has an orbital dependency not found in the usual KS equation. So, instead, we use the initial (non-SIC) NPA eigenfunction as an approximate estimate of $\Delta\epsilon_{sic}$. Furthermore, as we use a spin-unpolarized representation, $n_{\alpha,\sigma} = n_{\alpha}/2$. The zero- T form of the electron XC functional or its finite- T form can be used with little error since the T/E_F in the range of study is less than unity for all densities except the lowest. In Fig. 3 we display the SIC-corrected \bar{Z} from the NPA, together with the TF and QMD data (without SIC). The curve marked ‘NPA+Friedel’ is the estimate if the Friedel sumrule is strictly imposed. It is this \bar{Z} that we use in the following calculations. Since the SIC correction is itself an approximation, we may regard the spread among the three NPA curves as a measure of the uncertainty in our estimate of \bar{Z} . This uncertainty is smaller than the offset between the NPA and QMD estimates. The effect of the SIC (band gap error) on the QMD \bar{Z} is likely to be of about the same magnitude as the SIC in

the NPA. Hence we conclude that the offset is most likely to arise from a deeper underlying physical difference.

We do not subscribe to the view of some investigators that \bar{Z} is devoid of physical meaning, and that it is a convenient fit parameter taking various values depending on the physical property investigated, be it the the conductivity, XRTS, the diffusion coefficient or the opacity etc. The \bar{Z} appears in the theory as a valid DFT quantum statistical concept, as a Lagrange multiplier for charge neutrality, while μ, T appear as Lagrange multipliers for the conservation of particle number and the total energy. The Kohn-Sham eigenfunctions and energies also have a meaning in that they are the eigenfunctions and eigenenergies of the non-interacting electrons used in the DFT model. The NPA is also a non-interacting atom constructed from the interacting ions and electrons of the system.

In all NPA calculations we use the one unique value of \bar{Z} that satisfies the atomic physics, the Friedel sum rule, and the f -sum rule, without ‘fitting’ to any physical property. It is given by an all-electron atomic physics calculation of the NPA which incorporates a sophisticated free energy calculation inclusive of many-body effects. This is essentially the \bar{Z} that results from a sophisticated ‘Saha’ calculation [13].

The atomic physics of the NPA defines a pseudopotential based on \bar{Z} , and a pair-potential. They are sufficient to define all the thermodynamic properties and linear transport properties of the system. The \bar{Z} is a unique value that applies to all the calculated properties at a given ρ, T . Optical properties that involve instantaneous positions (e.g., line broadening due to ion microfields) of particles, rather than time averaged thermodynamic properties, are outside its scope unless time-dependent methods are used [36]. That pair-potentials are sufficient for the DFT based NPA approach, and that no three-body and higher terms have to be additionally included (contrary to the method followed in semi-empirical effective medium theories), have been discussed and clarified in our recent publications [14, 24].

The Perdew-Zunger approach is not easily applied to energy-bands. Even so, one may expect that if the band-gap error in the DFT-MD calculation were corrected using the GW method, then a comparable down-shifting of the QMD estimate of \bar{Z} would occur. So, the offset between the two methods remains.

In our view, this difference in \bar{Z} arises from the fact that the NPA (as well as other well known AA models) treat a strictly *uniform fluid*, while the QMD treats highly anisotropic crystals that are thermally averaged over many configurations without any assumption of radial symmetry. The NPA, together with the Ornstein-Zernike equation (OZ) and HNC equations can construct an ion-ion XC-functional that can treat non-uniform structures. The electron-ion XC-functional needs to be included in such calculations. In practice, MD simulations using the NPA pair-potentials would be more practical in dealing with inhomogeneous systems, than using

integral equations. In QMD many ionic configurations are explicitly created and searched. In our NPA calculations what is obtained is the best possible *uniform liquid* structure even if it be metastable with respect to some lower-energy solid-state structures (e.g., fullerene structures of carbon, Coulomb crystals) that may be possible under a given set of ρ, T . In contrast, simulations using $N = 2n, n = 16$ atoms in the simulation cell may favour icosahedral, folded-graphite forms (e.g., fullerenes and nanotubes in certain ranges of densities) [31]. They may include Coulomb-crystals [32, 33] that minimize the energy via shell-filling. In the following we present physical properties that support the view that the carbon system revealed by the QMD study may well be a dispersed complex-solid phase very different from a uniform liquid.

IV. CONDUCTIVITY

If the simulations used in Ref. [7] were to generate an average over many anisotropic crystalline structures, with some components of the conductivity tensor σ having high values, while another principle tensor component is minimally conducting, then the averaged conductivity obtained in the KG-calculation will show a very low conductivity. Alternatively, if the QMD simulation leads to a granular fluid, then hopping conductivity between grains will be small compared to that of a uniform metallic fluid. The fluid-like states studied by the NPA should lead to a spherically symmetric σ with a high conductivity resulting from the estimated high \bar{Z} . The Ziman formula evaluation [34] is implemented within a spherically symmetric $S(k)$ and a radial (s -wave) pseudopotential.

One may also evaluate the static conductivity σ via the KG equation using the continuum solutions of the NPA model. These too would be for a uniform fluid. But they do not contain the scattering from the field ions correctly since the NPA (and other AA-like models) use a spherical cavity, rather than the actual $\rho(r) = \bar{\rho}g(r)$ in modeling the ion distribution. Hence we do not use the KG-estimate of σ from the NPA, and instead calculate the conductivity using the pseudopotential given in Eq. 6 as well as a structure factor generated directly from the NPA calculations.

The conductivity calculated for the uniform fluid is an order of magnitude higher than that from the QMD calculation, even though QMD has a higher \bar{Z} , and more free electrons. Unfortunately, only one value of the static conductivity seems to be reported in Ref. [7]. Interestingly, the KG estimates of the static conductivity for liquid Li which is also an ion with only a small $1s$ core shows a strong difference between the Ziman formula estimate and the QMD-KG estimate. In Ref. [37] we reported that the atomic physics obtained from the NPA agreed accurately with the atomic physics of the QMD calculation for Li at 0.6 g/cm^3 and $T = 4.5 \text{ eV}$, predicting identical XRTS profiles. But the static conductivities from QMD

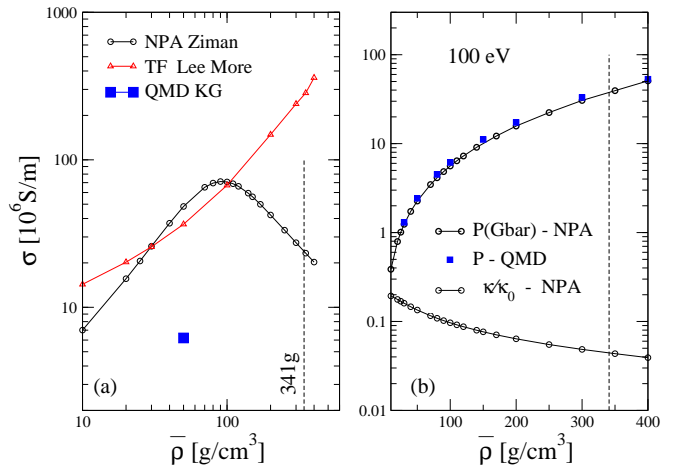


FIG. 4. (Color online) (a) The electrical conductivity of carbon evaluated using the NPA+Ziman formula, and using the TF-model of Lee and More [35]. A single QMD value is given. (b) The pressure and the microscopic compressibility κ in units of the ideal compressibility $1/Tr\bar{\rho}$. This is not derived from the pressure but taken from the $k \rightarrow 0$ limit of $S(k)$. The lack of discontinuities in the pressure or the compressibility rules out any phase transitions in the regime of $T, r\bar{\rho}$ studied. The QMD pressure, extracted from Fig. 4 of Ref. [7] is displayed. Given the higher free-electron content of QMD, the NPA pressure being slightly smaller is consistent.

and NPA-Ziman differed by a factor of five [38]. Lithium is also known to form complex structures. The calculation of the conductivity of liquid sodium near its melting point using the KG-formula is also subject to similar difficulties unless a very large number of particles is used in the simulation [39]. In the following we consider a particular model of a Coulomb crystal that may help to explain the reported results from QMD and AA models.

A. Coulomb crystals

The offset in \bar{Z} between the QMD result, and the results from homogeneous models (TF, Purgatorio, NPA) is $\sim \Delta\bar{Z} = 0.5$. Consider the carbon plasma at 50 g/cm^3 . It is very dense with $r_{ws} = 0.863, r_s = 0.4018 \text{ a.u.}$, and $\bar{Z} = 4.72, 4.19, 4.13,$ and 4.02 in QMD, TF, NPA and Purgatorio respectively. The QMD simulation treats 32 carbon atoms as a solid-state cluster. Since realistic first-principles potentials are being used, the usual properties of metallic clusters should apply to this simulation as well. More stable configurations are known as “magic numbers”, and this may arise from structural (packing) arrangements, and from electronic “shell filling” effects. The conditions for these ‘Coulomb crystals’ to form have been discussed by various authors [32], although exact conditions can be stated only in the context of various model systems. Results for hydrogenic systems, e.g., the condition for the Mott transition on $r_s \sim 1.2$, and similar

thresholds can be easily generalized to systems with \bar{Z} . Here we use results from actual calculations and experiments. The cluster has a nominal radius

$$R_{cl} = r_{ws} N^{1/3} = r_s \{\bar{Z}N\}^{1/3} \quad (9)$$

The equations to be solved are very similar to Eq. 3. The single nucleus at the center is replaced by a cluster of N -ions. In the simplest ‘jellium sphere’ approximation, this is equivalent to a spherical positive charge distribution of the form.

$$Q(r) = -\bar{Z}\rho(r) \quad (10)$$

$$\rho(r) = \frac{N}{2R_{cl}} \left[3 - \left(\frac{r}{R_{cl}} \right)^2 \right], \quad r \leq R_{cl} \quad (11)$$

$$= -\frac{N}{r}, \quad r > R_{cl}. \quad (12)$$

A more sophisticated form is obtained by introducing a self-consistently determined structure factor for the ions instead of using a jellium sphere. The \bar{Z} included in the above equations can be optimized in the usual manner, and is subject to the Friedel sum rule and the f sumrule. We do not solve this system as many results of solutions using DFT, as well as Quantum Monte Carlo results have been published [40]. Given that we are dealing with carbon, structures with $N = 4, 13, 55, 58$ are favoured structurally, with N being the number of ions. Electronic shell filling, determined by ‘‘jellium’’ magic numbers for the given number of electrons $n_e = \bar{Z}N$ is determined by the magic numbers 2, 8, 18, 20, 34, 36, 40, 54, 58, 68, 70, 86, 92, 106, 112, 138, 156, . . . , etc. Note that 156 electrons corresponds to about 31-32 carbon atoms with $\bar{Z} = 5$, or 39 atoms with $\bar{Z} = 4$.

The simulation may produce one, two or several clusters together with individual atoms among them as the MD simulation evolves. The mean density seen by each atom inside the cluster is quite oscillatory, and self-compressed by the surface energy of the cluster. The total energy is also an oscillatory function of N , and the structure arises from the Kohn-Sham solutions. For such systems, simulations with very large N are needed to achieve the properties of the homogeneous system. A small 4-atom carbon cluster, with a mean ionization $\bar{Z} = 4$ has $n_e = 16$, and hence achieves the magic number 18 if it acquires two more electrons and achieves a mean ionization of 4.5, thus registering the offset of $\Delta Z = 0.5$ seen in the QMD cluster calculation versus the uniform-density AA calculations. Such electrons occupy orbitals weakly localized on the cluster, and such electrons can contribute weakly to the conductivity by electron hopping from cluster to cluster. The fact that the simulation is done with periodic boundary conditions does not change this physical picture.

Many other clusters are possible as there is a choice of magic electron numbers as well as structural numbers that can combine to give specially stable structures, at any density in the range explored, with the 32-atom, or 64-atom QMD simulation. A 13-atom cluster may have atoms charged $\bar{Z} = 4$, having a total of 52 electrons, and acquire another 6 electrons to achieve the electron magic number 58. Such a structure is *both* structurally and electronically at a magic number, and conforms to HCP, FCC or icosahedral atomic arrangements. The extra 6 electrons added to complete the ‘magic shell’ will produce an offset $\Delta\bar{Z}=6/13=0.46$. One may identify a number of other such likely candidates stabilized by magic-number effects. All these structures may occur in a DFT-MD simulation and they would have lower energies than the uniform-fluid solution unless N were very large.

When very large numbers of particles, e.g. $N=1000$ are used in a simulation, the effect of such ‘magic clusters’ begins to average out, and bulk-like behaviour is reached. The physics described by Eq. 10 will approach that of the uniform ‘liquid-drop model’ as $N \rightarrow \infty$ and the oscillatory behaviour will disappear. Hence we may conclude that large QMD solutions will show a much smaller offset between the NPA (AA) predictions, and QMD predictions, both for \bar{Z} , and for the conductivity. On the otherhand, the offset between the QMD results and the average-atom results may persist, even when the N in the QMD simulations is significantly increased, indicating that carbon at 100 eV, at Gbar pressures does not exist as a uniform fluid of individual carbon ions.

V. CONCLUSION

A study of the properties of highly compressed hot carbon using the ‘single-atom’ DFT approach used in the neutral-pseudo atom model was undertaken to estimate the extent of self-interaction effects in this class of plasma models. It was concluded that the offset in the estimated number of free electrons, \bar{Z} between the average-atom estimate and the DFT-MD estimate *cannot* be explained by self-interaction errors. The extremely low conductivity predicted by the DFT-MD-KG calculations, in comparison to results from the Ziman formula and from the Lee-More formula strongly suggests that the DFT-MD simulations using 32 to 64 atoms differed from the average-atom models because the latter addressed only uniform-fluid solutions. The possible existence of ‘magic-number’ stabilized clusters is hypothesized to be a likely explanation of the observed differences between the 32 – 64-atom DFT-MD simulations, and effective ‘one-atom’ DFT simulations used in the NPA and Purgatorio codes.

- [2] G. Kresse and J. Furthmüller, Phys. Rev. B **54**, 11169 (1996).
- [3] X. Gonze and C. Lee, Computer Phys. Commun. **180**, 2582-2615 (2009).
- [4] L. Li, R. G. Parr, The Journal of chemical physics, **84**, 1704 (1986).
- [5] R. F. W. Bader, *Atoms in Molecules - A Quantum Theory*, Oxford University Press, Oxford, (1990)
- [6] K-U Plageman, H. R. Rüter, T. Bornath, Mohammed Shihab, Michael P. Desjarlais, C. Fortmann, S. Glenzer, R. Redmer, Phys. Rev. E **92**, 013103 (2015).
- [7] Mandy Bethkenhagen, Bastian B. L. Witte, Maximilian Schörner, Gerd Röpke, Tilo Döppner, Dominik Kraus, Siegfried H. Glenzer, Philip A. Sterne, and Ronald Redmer, Phys. Rev. Research **2**, 023260 (2020)
- [8] J. P. Perdew and Alex Zunger Phys. Rev. B **23**, 5048 (1981)
- [9] M. A. Hybertsen and S. G. Louie, Phys. Rev. Lett., **55**, 1418 (1985)
- [10] M. W. C. Dharma-wardana and F. Perrot, Phys. Rev. A **26**, 2096 (1982)
- [11] F. Perrot, Phys. Rev. E **47**, 570 (1993).
- [12] E. K. U. Gross, and R. M. Dreizler, *Density Functional Theory*, NATO ASI series, **337**, 625 Plenum Press, New York (1993).
- [13] F. Perrot and M.W.C. Dharma-wardana, Phys. Rev. E. **52**, 5352 (1995).
- [14] M. W. C. Dharma-wardana, Physics of Plasmas, (to be published) arXive preprint, cond-mat:2102.11112 (2021)
- [15] J. Chihara, Progr. Theor. Phys. Jpn. **59**, 1085 (1978).
- [16] R. Evans, Adv. Phys. **28**, 143 (1979).
- [17] F. Perrot, Y. Furutani and M.W.C. Dharma-wardana, Phys. Rev. A **41**, 1096-1104 (1990)
- [18] F. Perrot and M. W. C. Dharma-wardana, in *Radiative properties of hot dense matter*, 2nd Int. Conf. on rad. properties of hot dense matter. Eds. J. Davis, C. Hooper and R. Lee. World Scientific, Singapore. (1983)
- [19] F. Perrot and M. W. C. Dharma-wardana, Phys. Rev. A **29**, 1378 (1984)
- [20] Lucas J. Stanek, Raymond C. Clay III, M.W.C. Dharma-wardana, Mitchell A. Wood, Kristian R.C. Beckwith, Michael S. Murillo, Phys. Plasmas **28**, 032706 (2021). <https://arxiv.org/abs/2012.06451>
- [21] M.W.C. Dharma-wardana, Dennis D. Klug, and Richard C. Remsing. Phys. Rev. Lett. **125**, 075702 (2020). doi: 10.1103/PhysRevLett.125.075702
- [22] F. Perrot and M. W. C. Dharma-wardana, Phys. Rev. B **62**, 16536 (2000); *Erratum*: **67**, 79901 (2003); arXive-1602.04734.
- [23] Tobias Dornheim, Simon Groth, Michael Bonitz Physics Reports, **744**, 1-86 (2018), <https://doi.org/10.1016/j.physrep.2018.04.001>.
- [24] M. W. C. Dharma-wardana, Phys. Rev. B **100**, 155143 (2019) DOI: 10.1103/PhysRevB.100.155143
- [25] Pedro Borlido, Jonathan Schmidt, Ahmad W. Huran, Fabien Tran, Miguel A. L. Marques and Silvana Botti, Computational Materials **6**, Article number: 96 (2020).
- [26] R.M. More, K.H. Warren, D.A. Young, and G.B. Zimmerman, Phys. Fluids **31**, 3059 (1988).
- [27] J. P. Perdew, K. Burke, and M. Ernzerhof, Phys. Rev. Lett. **77**, 3865 (1996).
- [28] J. Sun, B. Xiao, Y. Fang, R. Haunschild, P. Hao, A. Ruzsinszky, G. I. Csonka, G. E. Scuseria, and J. P. Perdew, Phys. Rev. Lett. **111**, 106401 (2013).
- [29] Richard C. Remsing, Michael L. Klein and Jianwei Sun, Physical Review B **96**, 024203 (2017).
- [30] P.A. Sterne, S.B. Hansen, B.G. Wilson, W.A. Isaacs, High Energy Density Phys. **3**, 278 (2007).
- [31] A. Maiti, C. J. Brabec, and J. Bernholc, Phys. Rev. Lett. **70**, 3023 (1993).
- [32] M. Bonitz, P. Ludwig, Baumgartner, C. Henning, A. Filinov, D. Block, O. Arp, A. Piel, S. Käding, Y. Ivanov, A. Melzer, H. Fehske, and V. Filinov Physics Of Plasmas **15**, 055704 (2008).
- [33] Michael Drewsen, Physica B **460**, 105-113 (2015).
- [34] F. Perrot, M.W.C. Dharma-wardana, Phys. Rev. A **36**, 238-246 (1987).
- [35] Y. T. Lee and R. M. More, Phys. Fluids **27**, 1273 (1984).
- [36] F. Grimaldi, A. Lecourt-Grimaldi and M.W.C. Dharma-wardana, Phys. Rev. A **32**, 1063 (1985).
- [37] M.W.C. Dharma-wardana, D. D. Klug, L. Harbour, Laurent J. Lewis, Phys. Rev. E **96**, 053206 (2017)
- [38] Witte, B. B. L., and Shihab, M. and Glenzer, S. H. and Redmer, R. Phys. Rev. B, **95**, 144105 (2017).
- [39] Monica Pozzo, Michael P. Desjarlais, and Dario Alfè, Phys. Rev. B, **84**, 054203 (2011).
- [40] F. Sottile and P. Ballone, Phys. Rev. B **64**, 045105 (2001).